ACS APPLIED MATERIALS & INTERFACES

Research Article

www.acsami.org

Exoelectrogens Leading to Precise Reduction of Graphene Oxide by Flexibly Switching Their Environment during Respiration

Prerna Bansal,[†] Sejal Doshi,[‡] Ajay S. Panwar,[§] and Dhirendra Bahadur*

Department of Metallurgical Engineering and Materials Science, IIT Bombay, Mumbai 400076, India

Supporting Information

ABSTRACT: Reduced graphene oxide (RGO) has been prepared by a simple, cost-effective, and green route. In this work, graphene oxide (GO) has been reduced using Gram-negative facultative anaerobe *S. dysenteriae*, having exogenic properties of electron transfer via electron shuttling. Apparently, different concentrations of GO were successfully reduced with almost complete mass recovery. An effective role of lipopolysaccharide has been observed while comparing RGO reduced by *S. dysenteriae* and *S. aureus*. It was observed that the absence of lipopolysaccharide in Gram-positive *S. aureus* leads to a disrupted cell wall and that *S.aureus* could not survive in the presence of GO, leading to poor and inefficient reduction of GO, as shown in our results. However, *S. dysenteriae* having an outer lipopolysaccharide layer on its cell membrane reduced GO efficiently and the reduction process was extracellular for it. RGO prepared in our work has been characterized by X-ray diffraction, ζ potential, X-ray photoelectron spectroscopy, and Raman spectroscopy techniques, and the results were found to be in good agreement with those of chemically reduced GO. As agglomeration of RGO is the major issue to overcome while chemically reducing GO, we observed that RGO prepared by a bacterial route in our work has ζ potential value of −26.62 mV, good enough to avoid restacking of RGO. The role of exoelectrogens in electron transfer in the extracellular space has been depicted. Toxin released extracellularly during the process paves the way for reduction of GO due to its affinity towards oxygen.

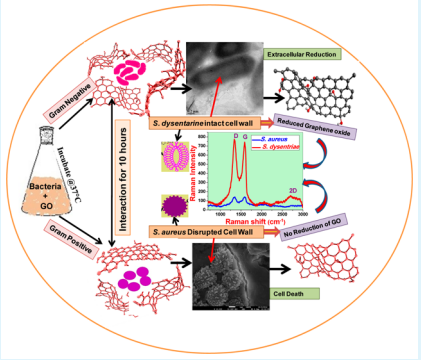

KEYWORDS: *graphene, biosynthesis, bacterial reduction, reduced graphene oxide, Shigella dysenteriae, mass production, green methodology*

1. INTRODUCTION

Graphene is an adept material with applications ranging from electronics to biosensors. This 2D sheet of carbon atoms has outstanding electronic,[1] mechanical,[2] thermal,[3] and optical properties[4] which make it useful in a wide spectrum of applications. Mass production of graphene in a cost-effective manner has been a major challenge for utilizing the full potential of this excellent material. For mass production of graphene, some alternative approaches need to be developed, as the chemical synthesis route involves use of hazardous and carcinogenic chemicals[5,6] and high temperatures.[7] Among many top down and bottom up approaches to produce graphene and its derivatives,[4−19] graphite oxidation−reduction has emerged as a better approach in terms of a high yield and low cost process.[6,12,13,17] Photocatalytic[20] and electrochemical methods,[21] UV radiation,[22] and use of Vitamin C,[23] sugar,[24] glucose,[25] green tea,[26] and cross-linking polymers[27] have also been reported for reduction of graphene oxide (GO). Reduction of GO using bacteriorhodopsin under irradiation was also reported.[28]

Recently, microorganisms[29−34] have been used as a green route for reduction of GO. Such biological paths have shown some promising results for GO reduction. It has been reported that the *Shewanella* cells can reduce GO through an electron transfer process mediated by cytochromes MtrA-C/OmcA.[29−31] In another study, GO sheets support growth of *E. coli* as biocompatible sites, while reduced graphene oxide (RGO) sheets were found to be a growth inhibitor for *E. coli*.[32,33] RGO nanowalls were found to be more toxic to the bacteria than the unreduced GO nanowalls.[35] Nonpathogenic extremophilic bacteria has also been used for GO reduction.[34] GO has been reported as an enhancer of cellular growth by helping cell proliferation.[36] Trapping of bacteria by RGO and its inactivation has also been reported.[37] Interaction of GO with common human gut bacteria *B. adolescentis* indicated that GO sheets promoted its proliferation, indicating good biocompatibility of GO.[38]

Such reports indicate that GO has been reduced using bacterial cells/biomass such as *Shewanella*[29−31] and *E. coli*.[32,33] However, there are clear gaps and many unsolved issues associated with reduction of GO through the bacterial route. Some of these issues include the importance of the bacterial cell membrane, less time consumption, maximum material yield, the role of the extracellular environment during interaction of bacterial cells with GO, and cost-effective mass production of high quality RGO, which have not been addressed clearly so far.

Received: May 20, 2015
Accepted: August 19, 2015
Published: August 19, 2015

DOI: 10.1021/acsami.5b04390
ACS Appl. Mater. Interfaces 2015, 7, 20576−20584

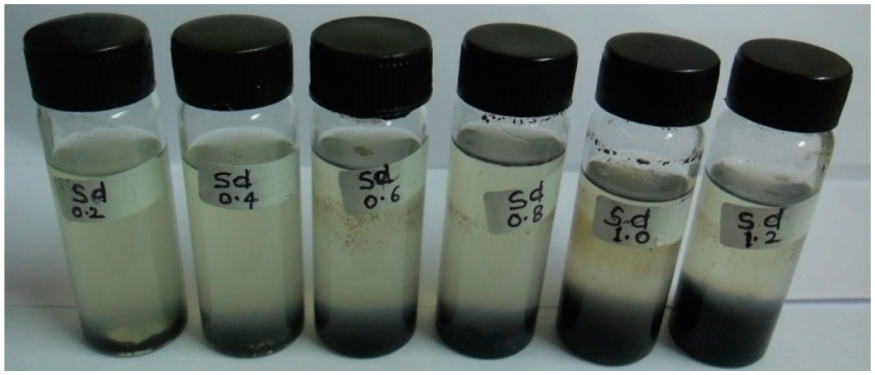

Figure 1. As-synthesized *Br*-RGO for different GO concentrations (0.2−1.2 mg/mL) in the presence of *S. dysenteriae* (*Sd*).

The present work is an attempt to answer these concerns and to bridge the gaps for achieving GO reduction by a green biological route using bacterial cells. Also, so far GO is reduced using anaerobic bacteria; hence, this work solves a fruitful purpose of using an aerobic environment to reduce GO.

We have observed that Gram-negative *Shigella dysenteriae* (*Sd*) has never been used for GO reduction until now. *Sd* is a Gram-negative coccobacilli.[39] Due to its facultative nature, it can flexibly change its respiratory environment from aerobic to anaerobic, thus having a tendency to survive for longer duration, which may be advantageous while using it for GO reduction. It was chosen as a model for GO reduction via electron shuttling and an extracellular electron transport mechanism. *Sd*, when present in water, causes severe dysentery, a pathogenic disease like shigellosis, with shiga toxin[40] being the causative agent, but herein, shiga toxin shall be used for GO reduction, avoiding use of harsh chemicals. Shiga toxin present in the periplasmic space of the *Sd* cells plays an important role in the electron transportation along with the cytochrome *bd oxidase* hooked on the outer membrane of the bacterial cell.[41] Being a Gram-negative bacteria, *Sd* has an advantage due to the presence of a lipopolysaccharide layer in its outer cell membrane while a Gram-positive bacterial cell wall like *S. aureus* (*Sa*) lacks this layer. These capacities of *Sd* motivated us to use it for the first time, as a novel model for studying the concerns related to biological approaches for reduction of GO. *Sd* is known to be a human pathogen, but the strain used in our work is of laboratory standards.

Further, a comparative study was endeavored using Gram-negative *Sd* and Gram-positive *Sa*. We observed that lipopolysaccharide holds responsibility for survival of Gram-negative bacterial cells in the presence of GO. Our bacterially-reduced graphene oxide (*Br*-RGO) samples were analyzed by X-ray diffraction (XRD), ζ potential, X-ray photoelectron spectroscopy (XPS), Fourier transform infrared spectroscopy (FTIR), and Raman spectroscopy techniques, and the results for *Br*-RGO samples were found to be in good agreement with the reported results for chemically synthesized RGO.[5,6,13]

2. MATERIALS AND METHODS

2.1. Synthesis of graphite oxide. An improved Hummer's method[12] was followed to oxidize pure graphite flakes (Sigma-Aldrich, 45 μm, 99.99%). For this, a 9:1 mixture of concentrated H_2SO_4/H_3PO_4 (60:6.66 mL) was added to a mixture of graphite flakes (500 mg, 1 wt equivalent) and $KMnO_4$ (3.0 g, 6 wt equivalent), producing a slight exotherm to 45−55 °C. This reaction was again heated at 55 °C with continuous stirring for 12 h. The reaction mixture was then cooled to room temperature and kept in an ice bath with 30% H_2O_2. After cooling, the obtained solution was filtered using nylon filter paper (0.2 μm pore size), using a vacuum filtration assembly. The residue was washed with water, 30% HCl, and ethanol alternately for several times. Later, the obtained material was coagulated with diethyl ether and filtered. It was then vacuum-dried at 60 °C overnight, which gave approximately 1g of graphite oxide powder. For the bacterial reduction of GO, a graphite oxide aqueous suspension (0.1 mg/mL) was prepared by sonicating graphite oxide powder (1 mg) in 10 mL of sterile distilled water for 1 h until a homogeneous brown dispersion was obtained. For mass reduction of GO, different concentrations (0.2 mg/mL−1.2 mg/mL) were prepared using a similar protocol.

2.2. Preparation of bacterial inoculum and reduction of GO. Bacterial strains of *Sd* and *Sa* were procured from K. C. College, Mumbai, India. These cultures were initially inoculated from patients infected with the respective bacteria. They have been subcultured since the past few years and hence assumed to have the least virulence. Nutrient broth media was procured from Himedia.

2.2.1. Growth curve. *Sd* and *Sa* were studied to obtain the mid-log phase. Mid-log phase refers to the period during which bacteria in culture are dividing rapidly and the cell density of the culture increases many fold. It is that stage of log-phase or exponential phase where cell division is at its peak, ready for any reaction. Briefly, 5 mL of overnight grown culture of *Sd* and *Sa* was added to an individual flat bottom conical flask containing 100 mL of autoclaved nutrient broth and incubated at 37 °C in an orbital shaker at 200 rpm. Periodically, OD was measured at 540 nm after every 5 min.

2.2.2. Reduction of GO. Overnight grown cultures of *Sd* and *Sa* were inoculated in 9 mL of sterile nutrient broth in sterile glass bottles individually. The control was sterile nutrient media to check for sterility of media and *Sd* and *Sa* inoculated in nutrient media individually. On acquiring the mid-log phase as calculated before, dispersed GO was added to the culture grown up to its exponential growth phase and incubated at 37 °C on an orbital shaker at 200 rpm for 10 h. All experiments were performed in triplicate. *Br*-RGO was observed settled at the bottom of the glass bottle in nutrient media, indicating reduction of GO. This solution was centrifuged at 5000 rpm for 1 min, and the supernatant was decanted. *Br*-RGO so obtained was washed once with ethanol to remove any bacterial debris and centrifuged twice with water. The residue in the centrifuge tube was dried in a vacuum oven overnight at 60 °C, giving *Br*-RGO powder which was further used for different characterizations.

2.3. Materials characterization. The crystalline nature of GO and *Br*-RGO was measured by XRD using a Philips powder diffractometer (PW3040/60) with Cu Kα (1.5406 Å) radiation. Raman spectra were recorded using a LabRAM HR 800 micro-Raman microscope (514.5 nm argon laser). FTIR spectra were obtained with a JASCO spectrometer (6100 type-A). The ζ potential was measured with a ζ potential analyzer (DelsaNano Corp.) to analyze the surface charges. The morphology of GO and *Br*-RGO was analyzed with a high resolution transmission electron microscope (HRTEM) and with field emission gun scanning electron microscopy (FEGSEM). The selected area electron diffraction (SAED) pattern was observed by HRTEM. X-ray photoelectron spectroscopy (XPS) measurements

DOI: 10.1021/acsami.5b04390
ACS Appl. Mater. Interfaces 2015, 7, 20576−20584

were done to analyze the molecular bonding of as-synthesized GO and *Br*-RGO using an electron spectroscopy chemical analysis probe (MULTILAB, Thermo VG Scientific) with a monochromatic Al Kα radiation of energy ~1486.6 eV.

3. RESULTS AND DISCUSSION

3.1. Extracellular interaction and GO reduction by Gram-negative facultative anaerobe *Sd*. Here we present a reduction of 0.1 mg/mL GO by Gram-negative facultative anaerobe *Sd*. GO was added during the mid-log phase, and its spontaneous conversion to *Br*-RGO was observed. *Sd* in mid-log phase was achieved after 3 h on addition of overnight grown inoculum. The reaction mixture was incubated in an orbital shaker for 10 h at 200 rpm at 37 °C. Further, different concentrations of GO (0.2 mg/mL to 1.2 mg/mL) were added to *Sd* and incubated at 37 °C in an orbital shaker for 10 h at 200 rpm. Figure 1 shows different concentrations (0.2 mg/mL to 1.2 mg/mL) of *Br*-RGO reduced in the presence of *Sd*.

A visible color change of as-synthesized GO (brown) to *Br*-RGO (black) was observed settled at the bottom of the bottle in nutrient media. This color change from brown to black indicated the reduction of GO to *Br*-RGO. On the other hand, there was no visible color change seen in control experiments (Figure S1 in the Supporting Information) with nutrient broth media alone without any bacterial species. *Br*-RGO was recovered successfully after removal of the bacterial debris by multiple washing with ethanol and water. It was used for further characterization to ensure the quality of as-obtained *Br*-RGO.

Addition of GO to the grown culture during the mid-log phase holds significance, as the exponential growth phase is the most active phase of the bacterial growth cycle. At this stage, the cell mass and cell number in the cultured media increase exponentially with time and the cell population doubles at regular intervals of time. The growth of the cells depends on the presence of an ambient energy source in the form of nutrients and salts and the presence of dissolved oxygen in the system. In addition, this energy is used to produce new cells and for the maintenance of existing cells. In our work, other than the media components, GO also acts as an oxygen source for cellular growth, and that way, GO itself gets reduced. Also, we observed the simultaneous formation of thin layers of *Br*-RGO on the surface of the media at the air water interface during the experiment. Due to the aerobic environment, bacteria at the surface of the media also hold capacity to reduce GO as the bacteria present in the media. Hence, *Sd* is an apt model for GO reduction in the extracellular environment.

3.1.1. Raman spectra of Br-RGO reduced by Sd. Confocal Raman measurements were taken using a WiTec Alpha300 Confocal Raman microscope with 532 nm wavelength incident laser light using a 50× objective lens. For all the bacteria samples, measurements were taken at 5 mW incident laser power to avoid any damage to the sample caused by laser-induced heating.

Raman spectroscopy is a well-known technique to characterize crystal structure, disorder, and defects in graphene and related materials. One can determine the degree of reduction of GO by Raman spectra by the changes in relative intensity of the two prominent D and G peaks.[42,43] It is well-known that Raman spectra of pure graphite show a strong G peak at ~1570 cm^{-1} due to the first order scattering of the E_{2g} phonon of sp^2 carbon atoms.[43] A broadened D peak appears in the Raman spectra of graphite oxide at ~1350 cm^{-1}, due to the reduction in size of the in-plane sp^2 domains of graphite induced by the creation of defects and distortions of the sp^2 domains. It is common to all sp^2 carbon lattices and arises from the stretching of the C−C bond. Figure 2 shows the Raman spectra of

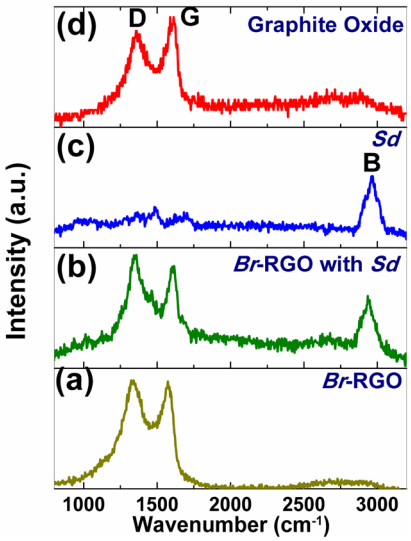

Figure 2. Raman spectra of (a) *Br*-RGO after removal of *Sd* cells, (b) *Br*-RGO in media before removal of *Sd* cells, (c) *Sd* cells in media, and (d) graphite oxide.

graphite oxide with the D peak at 1349 cm^{-1} and the G peak at 1581 cm^{-1}. The relative intensity ratio of both peaks (I_D/I_G) is a measure of disorder degree and is inversely proportional to the average size of the sp^2 clusters. The ratio of the D peak intensity to the G peak intensity (I_D/I_G) for graphite oxide is ~0.84. The I_D/I_G ratio for *Br*-RGO (reduced using *Sd*) is ~1.15. Such an increase in I_D/I_G for *Br*-RGO is in good agreement with the reported values of I_D/I_G for chemically synthesized RGO.[6] This suggests that more graphitic domains were formed and the sp^2 cluster number is increased post-reduction, indicating good reduction efficiency of *Sd*.[5,6]

The Raman spectra for *Br*-RGO in media before removal of *Sd* show D and G peaks similar to *Br*-RGO with an extra peak at ~2930 cm^{-1}. A similar peak is seen in the Raman spectra of *Sd* corresponding to the CH_3 symmetric stretch band near 2935 cm^{-1} (B peak), indicating the presence of phospholipids, which is a major constituent of the cell membrane.[44] A decrease is observed in the I_D/I_G ratio of *Br*-RGO after removal of the bacteria with ethanol, which might be due to reaction of ethanol with the residual oxygen functional groups of *Br*-RGO.

3.1.2. ζ Potential measurements of Br-RGO reduced by Sd. The surface charge (ζ potential) values (a) for *Sd* cells in media, (b) for *Br*-RGO before removal of *Sd* cells in media, (c) for *Br*-RGO after removal of *Sd* cells, and (d) for graphite oxide aqueous suspension at pH 6.8 ± 0.2 are presented in Figure 3.

The ζ potential value for *Sd* is −19.16 mV, which indicates that bacteria surfaces are negatively charged. We observed that aqueous suspension of graphite oxide is highly negatively charged (−38.18 mV), which is due to the ionization of the carboxylic acid and hydroxyl groups which are present on the edges and basal plane of the GO sheets.[5] The ζ potential value for *Br*-RGO without removal of bacterial debris was found to be (−20.47 mV), slightly more negative than that for *Sd*. We observed that the ζ potential value for *Br*-RGO increased after removal of bacterial debris with ethanol and water. The ζ potential value for *Br*-RGO (−26.62 mV) is lower than that for

DOI: 10.1021/acsami.5b04390
ACS Appl. Mater. Interfaces 2015, 7, 20576−20584

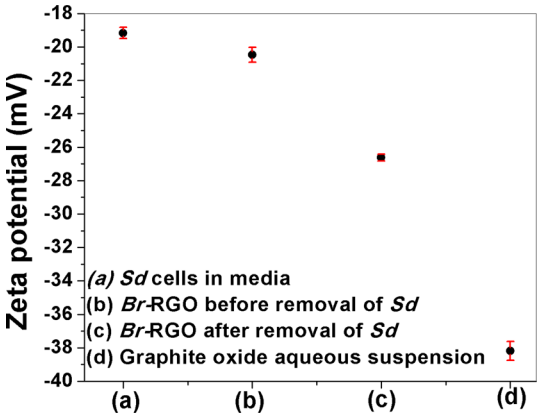

Figure 3. ζ Potential values for (a) *Sd* cells in media, (b) *Br*-RGO before removal of *Sd* cells in media, (c) *Br*-RGO aqueous suspension after removal of *Sd* cells, and (d) graphite oxide aqueous suspension.

GO (−38.18 mV) due to removal of oxygen functional groups after reduction by *Sd* cells. All the ζ potential values for graphite oxide, *Br*-RGO, and bacteria were in good agreement with their reported values for chemically synthesized RGO.[6] As agglomeration of RGO is a major issue to overcome while chemically reducing GO,[27] we observed that *Br*-RGO prepared by the bacterial route in our work has a ζ potential value (−26.62 mV) good enough to prevent restacking of *Br*-RGO.

3.1.3. FTIR measurement of Br-RGO reduced by Sd. Many distinct vibrational modes of various oxygen functionalities were observed in the Fourier-transform infrared (FTIR) spectra of graphite oxide and *Br*-RGO presented in Figure 4, recorded using KBr as reference. The FTIR spectra of graphite oxide showed a sharp broad peak of −OH stretching at nearly 3400 cm^{-1}, and a peak corresponding to bound H_2O molecules is observed at ~1363 cm^{-1}.

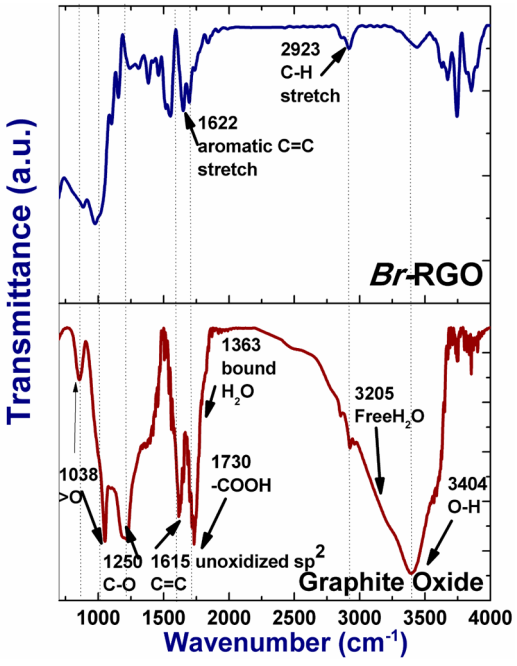

Figure 4. FTIR spectra of graphite oxide and *Br*-RGO reduced by *Sd* cells.

FTIR spectra of graphite oxide indicated graphite oxidation to a great extent, as confirmed by the presence of peaks corresponding to various oxygen functionalities such as −C═O (stretching of carbonyl and carboxyl groups at GO edges), C−O, and >O (epoxide) groups present at ~1730, ~1250, and ~1038 cm^{-1}, respectively. In-plane C═C bonds were seen to be present at ~1615 cm^{-1}. FTIR spectra of *Br*-RGO confirmed the efficient reduction of GO in the presence of *Sd*, indicated by a significant decrease in the intensity of peaks corresponding to various oxygen functionalities due to removal of partial carboxyl, hydroxyl, and epoxide groups from GO and also due to cracking of aromatic C═C bonds,[6] validating the reduction of functional groups by *Sd* cells. Also, C═C(aromatic stretch) and C—O were slightly shifted due to the change of the hydrophobic environment present in the reduced sample. Our FTIR result was found to be in good agreement with chemically synthesized RGO.[16]

3.1.4. HRTEM results: Extracellular GO reduction by Sd. Gram negative bacteria (*Sd*) has lipopolysaccharide in the outer part of its cell membrane whereas it is absent in Gram-positive bacteria (*Sa*). Figure 5a presents an HRTEM micrograph of control *Sd* cells in media, indicating an intact cell membrane. Figure 5b shows an HRTEM image of *Sd* after interaction with GO. It depicts that GO reduction by Gram-negative *Sd* is an extracellular process, as *Br*-RGO was found lying in the vicinity of the bacterial solution and the cell wall of the bacteria was intact. Various oxygen functional groups present in GO acted as a source of oxygen for the growth and maintenance of *Sd* cells. No damage was caused to *Sd* cells by GO. Hence, it was assumed that lipopolysaccharide may probably have a key role in extracellular interaction between Gram-negative *Sd* cells and GO. TEM results (Figure S2(b) in the Supporting Information) indicated a similar extracellular interaction between GO and *Sd*. The selected area electron diffraction (SAED) pattern of *Br*-RGO (Figure 5d) showed a hexagonally packed lattice whereas no diffraction spots or rings were seen for *Sd* bacteria, as expected.

3.1.5. XPS analysis of GO and Br-RGO reduced by Sd. To understand the extent of GO reduction through the bacterial route, XPS analysis was performed for GO and *Br*-RGO samples. To carry out XPS measurements, samples were drop cast on a Si substrate. Figure 6(a) presents the C1s spectra of GO, which is Gaussian fitted (using the software XPS Peak 4.1 with shirley background subtraction) as a superposition of four peaks at 284.8, 287.3, 289.6, and 282 eV. These peaks correspond to nonoxygenated ring carbon (C−C), carbonyl carbon (C═O), carboxylate carbon (O═C—OH), and C—Si, respectively (due to the Si substrate used for XPS measurements), indicating a considerable degree of oxidation of GO.

Figure 6(b) presents C1s XPS spectra for *Br*-RGO, indicating a significant reduction in the O/C fraction from ~2.4 for GO to ~0.42 for *Br*-RGO, due to a decrease in the peak intensity of the oxygen functional groups of GO. It shows efficient reduction of GO in the presence of *Sd*. For the hydrazine reduced GO, the O/C fraction is reported to vary from 0.21 to 0.09, depending upon the amount of hydrazine added and the time of contact with hydrazine.[45] We observed that post-reduction peak intensities for carbonyl carbon (C═O) at 287.3 eV and for carboxylate carbon (O═C−OH) at 289.6 eV were decreased to a great extent, indicating considerable deoxidation of GO by *Sd*. An increase in the intensity of the peak at 284.6 eV post-reduction indicated the restoration of sp^2 bonded

DOI: 10.1021/acsami.5b04390
ACS Appl. Mater. Interfaces 2015, 7, 20576−20584

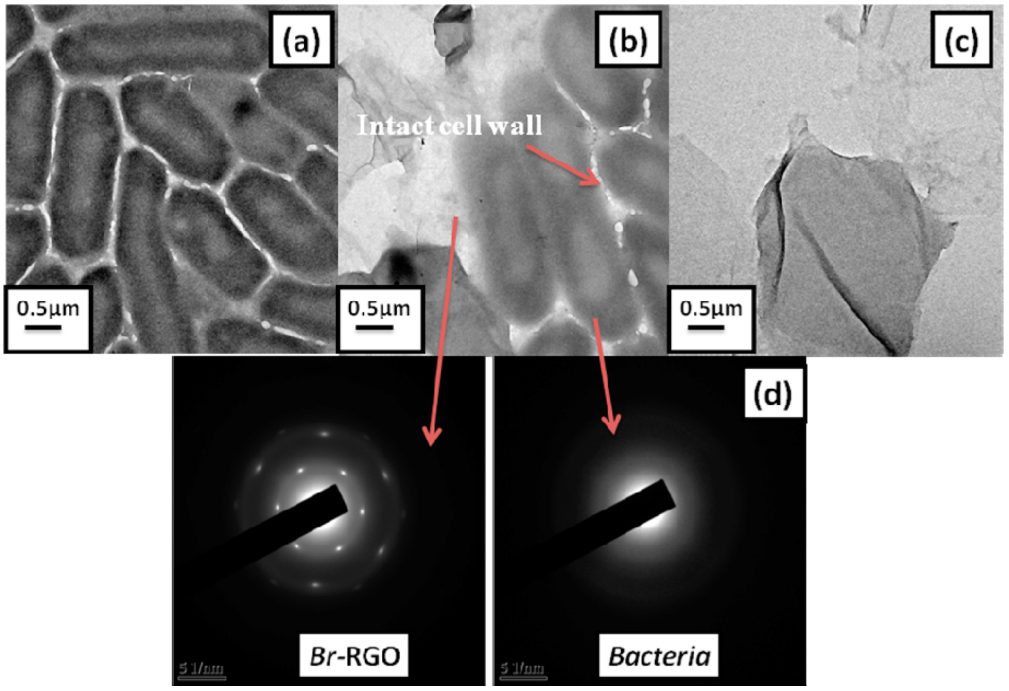

Figure 5. HRTEM images of (a) *Sd* cells, (b) *Sd* cells with *Br*-RGO sheets showing extracellular interaction, (c) *Br*-RGO sheets after removal of bacterial debris, and (d) diffraction patterns for *Br*-RGO and *Sd* bacteria cells, recorded for two different areas marked with arrows.

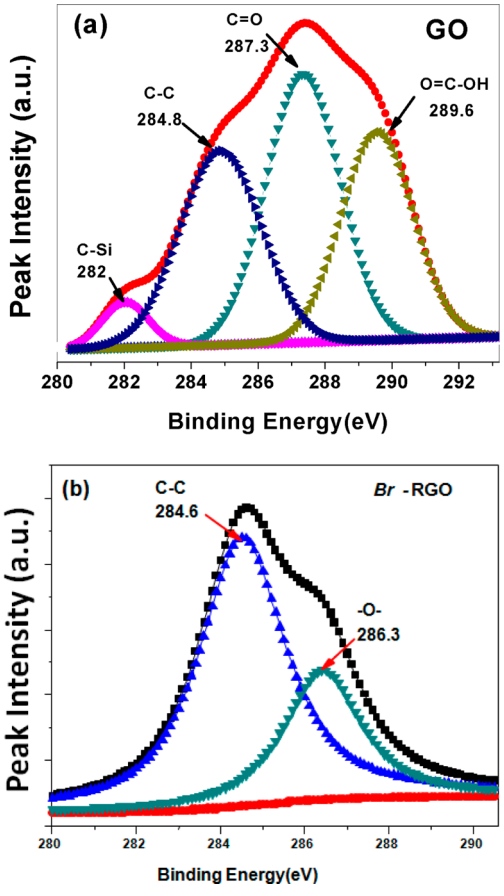

Figure 6. C1s XPS spectra of (a) GO and (b) *Br*-RGO.

carbon after reduction.[46] The analysis of the peak area ratio of four components of the C 1s spectra of GO confirmed that ~30% of carbon in GO is not bound to any oxygen functionality, while for *Br*-RGO the same is found to be ~70%. Such a decrease in the intensity of oxygen functionalities present in GO after interacting it with *Sd* is in good agreement with chemically synthesized RGO.[45−47] Our XPS results for GO and *Br*-RGO are in good accordance with our FTIR results indicating decrease in the O/C fraction upon reduction.

XRD results (Figure S3 in the Supporting Information) indicated a shift in the position of the [002] diffraction peak of GO from $2\theta \sim 9.56°$ to $2\theta \sim 23°$, indicating reduction of GO to *Br*-RGO by *Sd* cells.[6] Also, broadening of the [002] peak upon reduction indicated a decrease in the crystalline nature due to insertion of defects and distortions of the sp^2 lattice upon reduction. These results are well in agreement with our Raman studies, which indicated an increase in the I_D/I_G value for *Br*-RGO, leading to more defects. UV−vis absorption studies (Figure S4 in the Supporting Information) of pure GO and *Br*-RGO showed that upon reduction there is a significant red shift in the position of the peak at 230 nm for the *Br*-RGO sample in the absorption spectra which indicated the restoration of the electronic conjugation after reduction by *Sd* cells.[16]

3.1.6. Possible mechanism for GO reduction by Gram-negative Sd. Facultative anaerobes, especially Shigella *spps.*, have a tendency to switch respiration cycle, as the environment facilitates. Most likely they use the aerobic way of respiration, thus releasing 2 molecules of ATP. Nitrate reductase generates proton motive force, and ATP synthase bound to the membrane serves the physiological function of transforming electrochemical potential across the membrane, synthesizing ATP from ADP, with the help of an electrochemical gradient. Growth of new cells takes place actively during the exponential growth phase; cells require more and more energy from the available sources in their environment.

For this energy generation, cells consume oxygen from GO, and hence, GO itself gets reduced. On the other hand, the oxygen supply borrowed from GO plays a role in the electron

DOI: 10.1021/acsami.5b04390
ACS Appl. Mater. Interfaces 2015, 7, 20576−20584

transport chain, which oxidizes NADH and $FADH_2$ back to NAD+ and FAD+, which are involved in the four reduction reactions of the respiration cycle. In *Sd*, NADH is reduced to NAD+ in the presence of NADH reductase. The extracellular interaction between *Sd* and GO in the present work has been attributed to periplasmic toxin Shiga, as it has various receptor sites such as glycoconjugates that include oxygen.[48] In addition, cytochrome bd oxidase and aa3 oxidase equally contribute for electron transportation (as shown pictorially in Figure 7). The efficient energy of the aa3-type cytochrome c oxidase supercomplex yields the enzyme having greater affinity for oxygen.

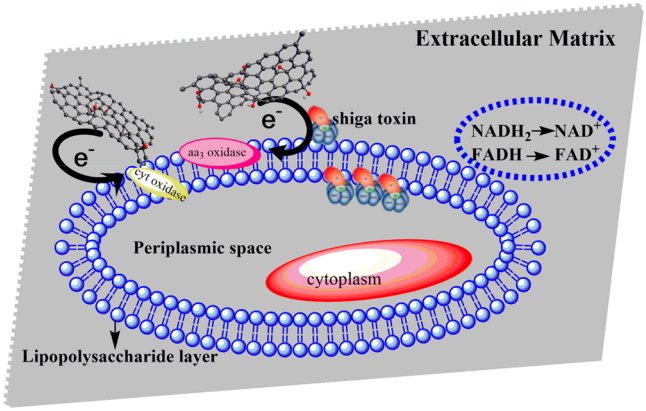

Figure 7. Possible mechanism for GO reduction in the presence of *Sd*.

3.2. GO interaction with Gram-positive *Sa*. It is well-known that Gram-negative bacteria have lipopolysaccharide in the outer part of the cell membrane whereas it is absent in Gram-positive bacteria. As seen in our results for Gram-negative *Sd*, the cell membrane was found intact after interaction with GO, indicating extracellular interaction between GO and Gram-negative *Sd*. To understand the role of the bacterial cell membrane, we have conducted a comparative study between Gram-negative and Gram-positive bacteria. In our work we have selected *Sa* as a model for Gram-positive cocci. While choosing the two model bacteria for our work, we took enough care to select species which belong to different genus; S in *Sd* stands for *Shigella*, whereas in *Sa*, it stands for *Staphylococcus*. This section presents our results related to GO interactions with Gram-positive *Sa*.

3.2.1. FEGSEM results: Interaction between GO and Sa. Figure 8 presents FEGSEM micrographs of a control image of *Sa* cells showing the intact cell membrane before its interaction with GO.

From our FEGSEM micrographs, presented in Figure 9(a,b), we observed a disrupted cell wall with spikes all around *Sa* after its interaction with GO, while for control *Sa* cells, presented in Figure 8(a,b), the bacterial cell membrane was found intact before interaction with GO. Such cell wall rupture seen for *Sa* cells after interaction with GO did not happen in our work with *Sd* cells (section 3.1.4). We found that, during reduction of GO, the outer surface of *Sa* was completely denatured, leading to cell death. This activity had occurred in *Sa* due to the absence of a lipopolysaccharide layer, unlike in the Gram-negative bacteria *Sd*.

Lipopolysaccharide (LPS) is a lipid bilayer present in the outermost part of Gram-negative bacterial cell membranes whereas it is absent in Gram-positive bacteria. It consists of lipids and polysaccharides joined together covalently. LPS mainly involves O antigen, core oligosaccharide, and lipid A.[49] The lipid A layer is well-known to act as an endotoxin and is, thus, responsible for the structural integrity and toxicity of Gram-negative bacteria. This layer makes the cell membrane more negatively charged, which leads to a more stabilized membrane structure protecting the Gram-negative cell membrane from specific chemicals. Due to an outer protecting lipopolysacharride layer, Gram-negative *Sd* survives in the presence of GO and leads to efficient GO reduction while the absence of a lipopolyscharride layer in Gram-positive *Sa* leads to cell death, as confirmed by our morphological studies.

Another point of notice was the growth rate of *Sa*, which was slower as compared to that of *Sd*. Thus, the time of interaction with GO for reduction was lower in case of *Sa*. Due to the deficiency of interaction between the oxygen molecule from GO and the molecular signal in the form of enzyme, a distinguished event has occurred in *Sa*, rendering it to be a weak tool for GO reduction.

Further, we observed that the bacterial morphology, either rod shaped (*Sd*) or spherical shaped (*Sa*), does not play any role in GO reduction, because whatever the shape, both the bacterial surfaces were negatively charged. The ζ potential

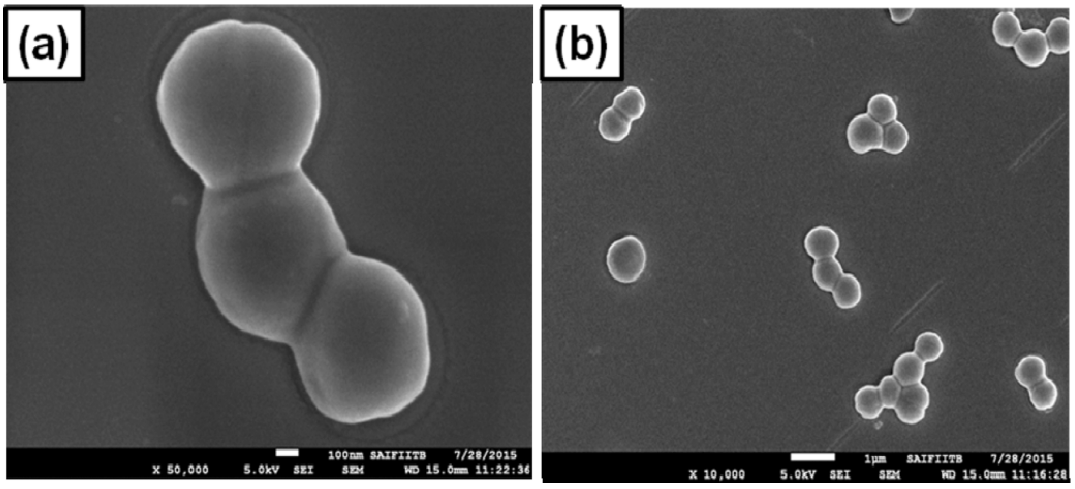

Figure 8. (a) and (b) FEGSEM image of *Sa* cells before interaction with GO (Images were taken at different magnifications).

DOI: 10.1021/acsami.5b04390
ACS Appl. Mater. Interfaces 2015, 7, 20576−20584

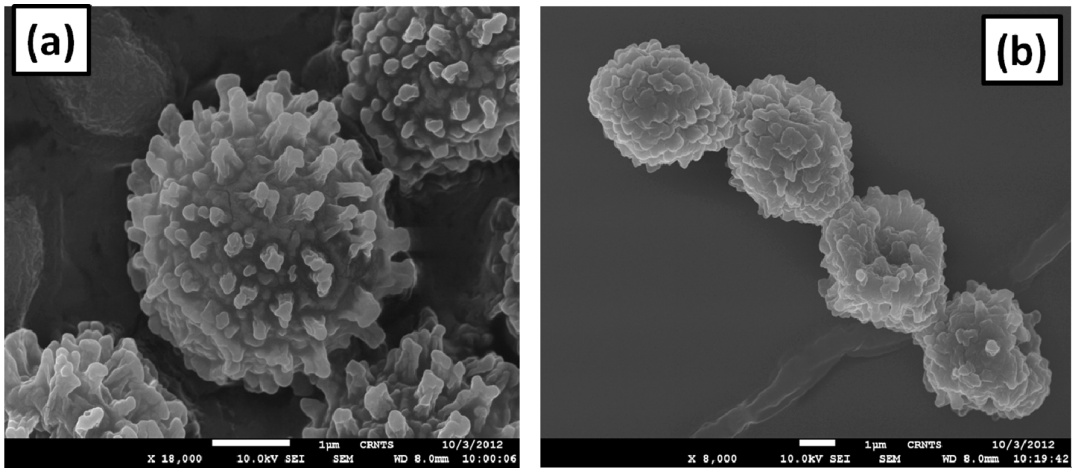

Figure 9. (a) and (b) FEGSEM images of Gram-positive bacteria *Sa* after interaction with GO (Images were taken at different magnifications).

values for *Sd and Sa* cells in media were found to be −19.16 mV and −18.95 mV, respectively. This indicates that the surface potentials were almost the same (−19 ± 0.5) for both the bacterial morphologies.

4. CONCLUSIONS

Efforts to produce an environmentally benign method for reduction of GO has been successfully achieved. Thereby, bacterial reduction of GO sturdily relies on the structure of the bacterial cell membrane, in particular, the lipopolyscharride layer beneath the outer membrane. Due to the availability of the lipopolyscharride layer under the outer membrane of Gram-negative bacteria (*Sd*), GO is reduced extracellularly. As the lipopolysaccharide layer is absent in Gram-positive bacteria (*Sa*), it could not survive in the presence of GO and reduction of GO was not achieved by it. Apparently, the bacterial morphology had no role in the reduction of GO through the bacterial route. It was observed that, if GO was added during the mid-log phase of the bacterial growth cycle, then *Br*-RGO formation was instant. The present investigation for GO reduction using *Sd* is a low cost, effective, easy, reproducible, and energy efficient method.

FTIR spectra of *Br*-RGO confirmed the efficient reduction of GO in the presence of *Sd*, indicated by a significant decrease in the intensity of peaks corresponding to various oxygen functionalities, due to removal of partial carboxyl, hydroxyl, and epoxide groups. XPS measurements performed on *Br*-RGO showed a significant reduction in the O/C fraction due to a decrease in the peak intensity of the oxygen functional groups, indicating efficient reduction of GO in the presence of *Sd*. The ζ potential value for *Br*-RGO (−26.62 mV) is lower than that of GO (−38.18 mV) due to removal of oxygen functional groups after reduction by *Sd* cells.

The above results lead to a path by which a microbe with redox potential has a promising impendence to reduce GO. It is now convincing to use bacteria available in the environment that cause nuisance in the form of dreadful diseases, for a good cause such as processing graphitic materials. With this study it is shown that lipopolysacharride along with exoelectrogens are responsible for reducing GO. Avoiding use of hazardous chemicals, and rather imbibing a green route to synthesize nanomaterials for mass production with consistent reproducibility, was the target achieved.

■ ASSOCIATED CONTENT

Supporting Information

The Supporting Information is available free of charge on the ACS Publications website at DOI: 10.1021/acsami.5b04390.

Control experiment: GO interaction with nutrient broth media (without any bacterial species); TEM results: Extracellular interaction between GO and *S. dysenteriae* cells; XRD spectra of *Br*-RGO; optical studies of bacterially reduced graphene oxide samples. (PDF)

■ AUTHOR INFORMATION

Corresponding Author

*Fax: +91 22 2572 3480. E-mail address: dhirenb@iitb.ac.in (D. Bahadur).

Present Addresses

†(P.B.) E-mail: prerna.bansal@iitb.ac.in.
‡(S.D.) E-mail: sejal.nanotech@iitb.ac.in.
§(A.S.P.) E-mail: panwar@iitb.ac.in.

Notes

The authors declare no competing financial interest.

■ ACKNOWLEDGMENTS

The authors would like to thank Nanomission-DST, Government of India, for providing financial support to conduct this research. Also, they greatly acknowledge the central characterization facilities at SAIF, IIT Bombay, India.

■ REFERENCES

(1) Geim, A. K.; Novoselov, K. S. The Rise of Graphene. *Nat. Mater.* **2007**, *6* (3), 183−91.
(2) Lee, C.; Wei, X.; Kysar, J. W.; Hone, J. Measurement of the Elastic Properties and Intrinsic Strength of Monolayer Graphene. *Science* **2008**, *321* (5887), 385−8.
(3) Balandin, A. A. Thermal Properties of Graphene and Nanostructured Carbon Materials. *Nat. Mater.* **2011**, *10* (8), 569−81.
(4) Li, X.; Cai, W.; An, J.; Kim, S.; Nah, J.; Yang, D.; Piner, R.; Velamakanni, A.; Jung, I.; Tutuc, E.; Banerjee, S. K.; Colombo, L.; Ruoff, R. S. Large-Area Synthesis of High-Quality and Uniform Graphene Films on Copper Foils. *Science* **2009**, *324* (5932), 1312−1314.
(5) Li, D.; Muller, M. B.; Gilje, S.; Kaner, R. B.; Wallace, G. G. Processable Aqueous Dispersions of Graphene Nanosheets. *Nat. Nanotechnol.* **2008**, *3* (2), 101−105.

DOI: 10.1021/acsami.5b04390
ACS Appl. Mater. Interfaces 2015, 7, 20576−20584

(6) Stankovich, S.; Dikin, D. A.; Piner, R. D.; Kohlhaas, K. A.; Kleinhammes, A.; Jia, Y.; Wu, Y.; Nguyen, S. T.; Ruoff, R. S. Synthesis of Graphene-Based Nanosheets via Chemical Reduction of Exfoliated Graphite Oxide. *Carbon* **2007**, *45* (7), 1558−1565.
(7) Wang, Z.-l.; Xu, D.; Huang, Y.; Wu, Z.; Wang, L.-m.; Zhang, X.-b. Facile, Mild and Fast Thermal-Decomposition Reduction of Graphene Oxide in Air and Its Application in High-Performance Lithium Batteries. *Chem. Commun.* **2012**, *48* (7), 976−978.
(8) Bae, S.; Kim, H.; Lee, Y.; Xu, X.; Park, J.-S.; Zheng, Y.; Balakrishnan, J.; Lei, T.; Ri Kim, H.; Song, Y. I.; Kim, Y.-J.; Kim, K. S.; Ozyilmaz, B.; Ahn, J.-H.; Hong, B. H.; Iijima, S. Roll-to-Roll Production of 30-Inch Graphene Films for Transparent Electrodes. *Nat. Nanotechnol.* **2010**, *5* (8), 574−578.
(9) Norimatsu, W.; Kusunoki, M. Epitaxial Graphene on SiC{0001}: Advances and Perspectives. *Phys. Chem. Chem. Phys.* **2014**, *16* (8), 3501−3511.
(10) Hernandez, Y.; Nicolosi, V.; Lotya, M.; Blighe, F. M.; Sun, Z.; De, S.; McGovern, I. T.; Holland, B.; Byrne, M.; Gun'Ko, Y. K.; Boland, J. J.; Niraj, P.; Duesberg, G.; Krishnamurthy, S.; Goodhue, R.; Hutchison, J.; Scardaci, V.; Ferrari, A. C.; Coleman, J. N. High-Yield Production of Graphene by Liquid-Phase Exfoliation of Graphite. *Nat. Nanotechnol.* **2008**, *3* (9), 563−568.
(11) Malik, S.; Vijayaraghavan, A.; Erni, R.; Ariga, K.; Khalakhan, I.; Hill, J. P. High Purity Graphenes Prepared by a Chemical Intercalation Method. *Nanoscale* **2010**, *2* (10), 2139−2143.
(12) Marcano, D. C.; Kosynkin, D. V.; Berlin, J. M.; Sinitskii, A.; Sun, Z.; Slesarev, A.; Alemany, L. B.; Lu, W.; Tour, J. M. Improved Synthesis of Graphene Oxide. *ACS Nano* **2010**, *4* (8), 4806−4814.
(13) Mao, S.; Pu, H.; Chen, J. Graphene Oxide and Its Reduction: Modeling and Experimental Progress. *RSC Adv.* **2012**, *2* (7), 2643−2662.
(14) Dreyer, D. R.; Ruoff, R. S.; Bielawski, C. W. From Conception to Realization: An Historial Account of Graphene and Some Perspectives for Its Future. *Angew. Chem., Int. Ed.* **2010**, *49* (49), 9336−9344.
(15) Georgakilas, V.; Otyepka, M.; Bourlinos, A. B.; Chandra, V.; Kim, N.; Kemp, K. C.; Hobza, P.; Zboril, R.; Kim, K. S. Functionalization of Graphene: Covalent and Non-Covalent Approaches, Derivatives and Applications. *Chem. Rev.* **2012**, *112* (11), 6156−6214.
(16) Cooper, D. R.; D'Anjou, B.; Ghattamaneni, N.; Harack, B.; Hilke, M.; Horth, A.; Majlis, N.; Massicotte, M.; Vandsburger, L.; Whiteway, E.; Yu, V. Experimental Review of Graphene. *ISRN Condens. Matter Phys.* **2012**, *2012*, 56.
(17) Esfandiar, A.; Akhavan, O.; Irajizad, A. Melatonin as a Powerful Bio-Antioxidant for Reduction of Graphene Oxide. *J. Mater. Chem.* **2011**, *21* (29), 10907−10914.
(18) Akhavan, O.; Bijanzad, K.; Mirsepah, A. Synthesis of Graphene From Natural and Industrial Carbonaceous Wastes. *RSC Adv.* **2014**, *4* (39), 20441−20448.
(19) Ruan, G.; Sun, Z.; Peng, Z.; Tour, J. M. Growth of Graphene from Food, Insects, and Waste. *ACS Nano* **2011**, *5* (9), 7601−7607.
(20) Akhavan, O.; Abdolahad, M.; Esfandiar, A.; Mohatashamifar, M. Photodegradation of Graphene Oxide Sheets by TiO2 Nanoparticles After a Photocatalytic Reduction. *J. Phys. Chem. C* **2010**, *114* (30), 12955−12959.
(21) Shao, Y.; Wang, J.; Engelhard, M.; Wang, C.; Lin, Y. Facile and Controllable Electrochemical Reduction of Graphene Oxide and Its Applications. *J. Mater. Chem.* **2010**, *20* (4), 743−748.
(22) Swain, A. K.; Li, D.; Bahadur, D. UV-Assisted Production of Ferromagnetic Graphitic Quantum Dots From Graphite. *Carbon* **2013**, *57* (0), 346−356.
(23) Fernández-Merino, M. J.; Guardia, L.; Paredes, J. I.; Villar-Rodil, S.; Solís-Fernández, P.; Martínez-Alonso, A.; Tascón, J. M. D. Vitamin C Is an Ideal Substitute for Hydrazine in the Reduction of Graphene Oxide Suspensions. *J. Phys. Chem. C* **2010**, *114* (14), 6426−6432.
(24) Zhu, C.; Guo, S.; Fang, Y.; Dong, S. Reducing Sugar: New Functional Molecules for the Green Synthesis of Graphene Nanosheets. *ACS Nano* **2010**, *4* (4), 2429−2437.
(25) Akhavan, O.; Ghaderi, E.; Aghayee, S.; Fereydooni, Y.; Talebi, A. The Use of a Glucose-Reduced Graphene Oxide Suspension for Photothermal Cancer Therapy. *J. Mater. Chem.* **2012**, *22* (27), 13773−13781.
(26) Wang, Y.; Shi, Z.; Yin, J. Facile Synthesis of Soluble Graphene via a Green Reduction of Graphene Oxide in Tea Solution and Its Biocomposites. *ACS Appl. Mater. Interfaces* **2011**, *3* (4), 1127−1133.
(27) Swain, A. K.; Bahadur, D. Enhanced Stability of Reduced Graphene Oxide Colloid Using Cross-Linking Polymers. *J. Phys. Chem. C* **2014**, *118* (18), 9450−9457.
(28) Akhavan, O. Bacteriorhodopsin as a Superior Substitute for Hydrazine in Chemical Reduction of Single-Layer Graphene Oxide Sheets. *Carbon* **2015**, *81* (0), 158−166.
(29) Salas, E. C.; Sun, Z.; Lüttge, A.; Tour, J. M. Reduction of Graphene Oxide via Bacterial Respiration. *ACS Nano* **2010**, *4* (8), 4852−4856.
(30) Wang, G.; Qian, F.; Saltikov, C.; Jiao, Y.; Li, Y. Microbial Reduction of Graphene Oxide by Shewanella. *Nano Res.* **2011**, *4* (6), 563−570.
(31) Jiao, Y.; Qian, F.; Li, Y.; Wang, G.; Saltikov, C. W.; Gralnick, J. A. Deciphering the Electron Transport Pathway for Graphene Oxide Reduction by Shewanella Oneidensis MR-1. *J. Bacteriol.* **2011**, *193* (14), 3662−3665.
(32) Akhavan, O.; Ghaderi, E. Escherichia Coli Bacteria Reduce Graphene Oxide to Bactericidal Graphene in a Self-Limiting Manner. *Carbon* **2012**, *50* (5), 1853−1860.
(33) Gurunathan, S.; Han, J. W.; Eppakayala, V.; Kim, J.-H. Microbial Reduction of Graphene Oxide by Escherichia Coli: A Green Chemistry Approach. *Colloids Surf., B* **2013**, *102* (0), 772−777.
(34) Raveendran, S.; Chauhan, N.; Nakajima, Y.; Toshiaki, H.; Kurosu, S.; Tanizawa, Y.; Tero, R.; Yoshida, Y.; Hanajiri, T.; Maekawa, T.; Ajayan, P. M.; Sandhu, A.; Kumar, D. S. Ecofriendly Route for the Synthesis of Highly Conductive Graphene Using Extremophiles for Green Electronics and Bioscience. *Particle & Particle Systems Characterization* **2013**, *30* (7), 573−578.
(35) Akhavan, O.; Ghaderi, E. Toxicity of Graphene and Graphene Oxide Nanowalls Against Bacteria. *ACS Nano* **2010**, *4* (10), 5731−5736.
(36) Ruiz, O. N.; Fernando, K. A. S.; Wang, B.; Brown, N. A.; Luo, P. G.; McNamara, N. D.; Vangsness, M.; Sun, Y.-P.; Bunker, C. E. Graphene Oxide: A Nonspecific Enhancer of Cellular Growth. *ACS Nano* **2011**, *5* (10), 8100−8107.
(37) Akhavan, O.; Ghaderi, E.; Esfandiar, A. Wrapping Bacteria by Graphene Nanosheets for Isolation From Environment, Reactivation by Sonication, and Inactivation by Near-Infrared Irradiation. *J. Phys. Chem. B* **2011**, *115* (19), 6279−6288.
(38) Chen, H.-q.; Gao, D.; Wang, B.; Zhao, R.-f.; Guan, M.; Zheng, L.-n.; Zhou, X.-y.; Chai, Z.-f.; Feng, W.-y. Graphene Oxide as an Anaerobic Membrane Scaffold for the Enhancement of *B. Adolescentis* Proliferation and Antagonistic Effects Against Pathogens *E. Coli* and *S. Aureus*. *Nanotechnology* **2014**, *25* (16), 165101−165110.
(39) Keusch, G. T.; Grady, G. F.; Mata, L. J.; McIver, J. The Pathogenesis of Shigella Diarrhea: I. Enterotoxin Production by Shigella Dysenteriae 1. *J. Clin. Invest.* **1972**, *51* (5), 1212−1218.
(40) Asakura, H.; Makino, S.; Kobori, H.; Watarai, M.; Shirahata, T.; Ikeda, T.; Takeshi, K. Phylogenetic Diversity and Similarity of Active Sites of Shiga Toxin (Stx) in Shiga Toxin-Producing *Escherichia Coli* (STEC) Isolates From Humans and Animals. *Epidemiol. Infect.* **2001**, *127* (1), 27−36.
(41) Lovley, D. R. The Microbe Electric: Conversion of Organic Matter to Electricity. *Curr. Opin. Biotechnol.* **2008**, *19* (6), 564−571.
(42) Prakash, A.; Bahadur, D. The Role of Ionic Electrolytes on Capacitive Performance of ZnO-Reduced Graphene Oxide Nanohybrids with Thermally Tunable Morphologies. *ACS Appl. Mater. Interfaces* **2014**, *6* (3), 1394−1405.
(43) Ferrari, A. C. Raman Spectroscopy of Graphene and Graphite: Disorder, Electron−phonon Coupling, Doping and Nonadiabatic Effects. *Solid State Commun.* **2007**, *143* (1−2), 47−57.

DOI: 10.1021/acsami.5b04390
ACS Appl. Mater. Interfaces 2015, 7, 20576−20584

(44) Krafft, C.; Neudert, L.; Simat, T.; Salzer, R. Near Infrared Raman Spectra of Human Brain Lipids. *Spectrochim. Acta, Part A* **2005**, *61* (7), 1529−1535.
(45) Pei, S.; Cheng, H.-M. The Reduction of Graphene Oxide. *Carbon* **2012**, *50* (9), 3210−3228.
(46) Boutchich, M.; Jaffré, A.; Alamarguy, D.; Alvarez, J.; Barras, A.; Tanizawa, Y.; Tero, R.; Okada, H.; Thu, T. V.; Kleider, J. P.; Sandhu, A. Characterization of Graphene Oxide Reduced Through Chemical and Biological Processes. *J. Phys.: Conf. Ser.* **2013**, *433* (1), 012001.
(47) Prakash, A.; Chandra, S.; Bahadur, D. Structural, Magnetic, and Textural Properties of Iron Oxide-Reduced Graphene Oxide Hybrids and Their Use for the Electrochemical Detection of Chromium. *Carbon* **2012**, *50* (11), 4209−4219.
(48) Lindberg, A. A.; Brown, J. E.; Strömberg, N.; Westling-Ryd, M.; Schultz, J. E.; Karlsson, K. A. Identification of the Carbohydrate Receptor for Shiga Toxin Produced by Shigella Dysenteriae Type 1. *J. Biol. Chem.* **1987**, *262* (4), 1779−85.
(49) Raetz, C. R. H.; Whitfield, C. Lipopolysaccharide Endotoxins. *Annu. Rev. Biochem.* **2002**, *71* (1), 635−700.

DOI: 10.1021/acsami.5b04390
ACS Appl. Mater. Interfaces 2015, 7, 20576−20584